RSC Advances

PAPER

View Article Online
View Journal | View Issue

Cite this: *RSC Adv.*, 2019, **9**, 18703

The effect of nanoencapsulation of ICG on two-photon bioimaging†

Anshu Kumari,[a] Kalpana Kumari[a] and Sharad Gupta *[ab]

Multiphoton imaging, a highly effective diagnostic technique, has recently gained widespread attention for early-stage cancer detection. Tremendous efforts have been dedicated to explore various types of exogenous contrast agents for improved signal-to-noise ratio of multiphoton imaging. Indocyanine green (ICG), the only U. S. FDA approved near-infrared chromophore, has been recently used as an exogenous contrast agent for two-photon bioimaging. Despite its great potential applications in clinical settings, the conventional delivery method of ICG has limited applications due to its poor cellular uptake and optical stability in its free form. Herein, we report the effect of nanoencapsulation of ICG on two-photon bioimaging. For this study, ICG was encapsulated within poly-L-arginine (PLA) based nanoparticles for the first time. These nanoparticles were found to be biocompatible and biodegradable as the major constituents were salts and PLA. These nanoparticles were spherical with a mean diameter of ~61 nm and exhibit higher photostability than free ICG. Additionally, nanoencapsulated ICG treated cells show enhanced contrast for two-photon bioimaging in comparison with its free form. In summary, nanoencapsulated ICG could serve as an exogenous chromophore for multiphoton imaging, which shows excellent delivery efficacy.

Received 27th April 2019
Accepted 7th June 2019

DOI: 10.1039/c9ra03152a

rsc.li/rsc-advances

1 Introduction

Molecular imaging has the potential to advance early-stage cancer detection, which results in successful cancer treatment and improved patient survival rates.[1] The use of exogenous contrast agents with the existing imaging modalities has improved the signal-to-noise ratio (SNR) and diagnostic ability. Especially, the use of the near-infrared fluorescence (NIRF) imaging probe has enabled researchers to study the deep-seated cellular inhomogeneities with an enhanced SNR.[2–5] Over the past few decades, multiphoton fluorescence imaging has received much attention due to its several advantages over NIRF imaging techniques.[6] It provides three dimensional (3D) imaging capability of living cells, especially in thick tissues (few hundred micrometers) with reduced photobleaching and photodamage to the nearby tissues.[7–9] However, the inclusion of exogenous imaging probe in multiphoton imaging could further enhance imaging contrast, sensitivity, and SNR.[10]

Among various available exogenous dye, indocyanine green (ICG) is the only U. S. Food and Drug Administration (FDA) approved NIRF imaging probe, which is used for various clinical applications.[11–16] Recently, the nonlinear excitation of the ICG to the second excited singlet (S_2) state has gained attention for various applications.[17,18] In this direction, our group had reported the nonlinear excitation of ICG molecules to S_2 state followed by direct relaxation to the ground (S_0) state. Due to this property ICG falls in the list of molecules that violate Kasha's rule.[19,20] Additionally, this property was used for two-photon (2P) bioimaging.[21] Despite its application as a 2P imaging chromophore, the conventional delivery of ICG has limitations such as poor cellular uptake and aqueous photostability, which limits its application. Incorporating ICG within a nanocarrier is a promising way to overcome the limitations of free ICG.

A broad array of nanoparticles (NPs) such as liposomes, polymers, metals, viral ghost, *etc.* have been used for the delivery of imaging probes.[3,22–32] However, the clinical applications of these nanocarriers are limited due to their non-biodegradability, and long and short-term toxicity. Despite much progress in NP development, there is an unmet need to fabricate biodegradable nanocarrier for the delivery of ICG. The fabrication of the nanocarriers from the biological amino-acids could offer a biodegradable and biocompatible nanocarrier. Poly-L-arginine (PLA) is the homopeptide of L-arginine, which has been used in medical applications for many centuries due to its cellular penetrating properties.[33–39] Additionally, it is a semi-essential amino-acid with various roles such as in cell metabolism, wound healing, protein synthesis, and it also shows antimicrobial and

[a]*Discipline of Biosciences and Biomedical Engineering, Indian Institute of Technology Indore, Indore, India-453552. E-mail: shgupta@iiti.ac.in; Tel: +91-732-4306743*

[b]*Metallurgy Engineering and Materials Science, Indian Institute of Technology Indore, Indore, India-453552*

† Electronic supplementary information (ESI) available. See DOI: 10.1039/c9ra03152a

antitumor activity.[40–45] In particular, owing to their favorable properties, NPs comprised of PLA have garnered considerable interest for delivery of small molecules.[46–48] Hence, the synthesis of ICG-PLA NPs would not only help in cellular delivery but also would improve the optical stability of ICG.

Here, we report the fabrication of ICG loaded PLA NPs (ICG-PLA NPs) and its effect on optical properties and multiphoton imaging ability of ICG for the first time. The fabrication of these NPs was done *via* a simple two-step self-assembly method. The *in vitro* cellular study suggests that both free and nanoencapsulated ICG get endocytosed within the cells. However, the significantly enhanced delivery of ICG was shown by ICG-PLA NPs in comparison with free ICG. Additionally, nanoencapsulated ICG treated cells show enhanced contrast for 2P bioimaging in comparison with free ICG. In conclusion, the ICG-PLA NPs are biocompatible and biodegradable, which could be used for improved 2P bioimaging.

2 Materials and methods

2.1 Materials

Poly-L-arginine (PLA, M_W > 70 000 Da, ~365 arginine unit, one HCl per residue) and ethylenediaminetetraacetic acid tetrasodium salt hydrate (EDTA), indocyanine green (ICG) and fluoromount mounting media were purchased from Sigma Aldrich (St. Louis, MO, USA) and used without any further purification. The stock solutions of the chemicals were prepared in de-ionized (DI) water (Millipore 18.2 MΩ, Sartorius system). HeLa cells were procured from the National Centre for Cell Science (NCCS) Pune, India. Fetal Bovine Serum (FBS), Dulbecco's Modified Eagle Medium (DMEM), penicillin–streptomycin, 0.25% trypsin-1 mM ethylenediaminetetraacetic acid (EDTA) and 2.5% trypsin without phenol red were procured from Gibco, Thermo Fisher Scientific. 3-(4,5-Dimethylthiazol-2-yl)-2,5-diphenyltetrazolium bromide (MTT) was procured from Himedia (India).

2.2 Synthesis and characterization of the ICG-PLA NPs

The schematic representation of the fabrication process is illustrated in Fig. 1. The ICG-PLA NPs were prepared through a simple two-step self-assembly process. Briefly, 10 μL of PLA solution (2 mg mL^{-1}) was gently mixed with the 4 μL of the EDTA salts (0.1 M) for 20 seconds. Immediately after the mixing, the clear solution turns turbid which indicates the initiation of the nucleation process. Followed by the addition of the 250 μL of the ICG (645 μM) to the colloidal solution. Then the 1 mL of DI water was added to the suspension and aged for 1 hour to form ICG-PLA NPs. The systematic mixing of these precursors results in the fabrication of the ICG-PLA NPs.

The final NPs solution was collected by the differential centrifugation technique to get monodisperse NPs. The morphological study of the ICG-PLA NPs was done using a field-emission scanning electron microscope (FESEM, Carl Zeiss Sigma Series, Supra-55) equipped with energy dispersive X-ray spectroscopy (EDS, Oxford Instruments, X-MAX, 51-XMX1025). A secondary electron image (SEI) was taken under 3 kV electron beam with a working distance of ~12 mm. FESEM samples were prepared after the lyophilization of the ICG-PLA NPs pellet in a lyophilizer (Alpha 1-2 LD plus, Labmate). Following lyophilization, samples were placed on a double-sided carbon tape mounted on an aluminum stub. Before visualization in FESEM, the samples were sputter coated with gold by direct current (DC) sputter coater (Quorum (Q-150RES)) for better electron conductivity. The subsequent SEM images were analyzed using ImageJ software (National Institutes of Health, Bethesda, MD, U.S.A.). Dynamic light scattering (DLS) measurements were performed on a laser light scattering spectrometer (NanoPlus-3, Micromeritics) equipped with a diode laser (660 nm), and the geometry for collecting scattering light signals was at 175° for particle size analyzer and 45° for ζ potential measurements. Further, the zeta potential was also measured by DLS instrument. All the samples were measured at least three times at 25 °C in DI water.

2.3 Spectroscopic analysis

To investigate the encapsulation of the ICG, steady-state absorption of free ICG and ICG-PLA NPs was measured by UV-Vis-NIR spectrometer (Lambda-35, PerkinElmer). The absorption data were collected with 1 nm slit width and 480 nm min^{-1} scan rate. Further, the fluorescence emission spectra of free ICG and ICG-PLA NPs were also measured using spectrofluorimeter (FL3-21, Jobin Yvon, Horiba)

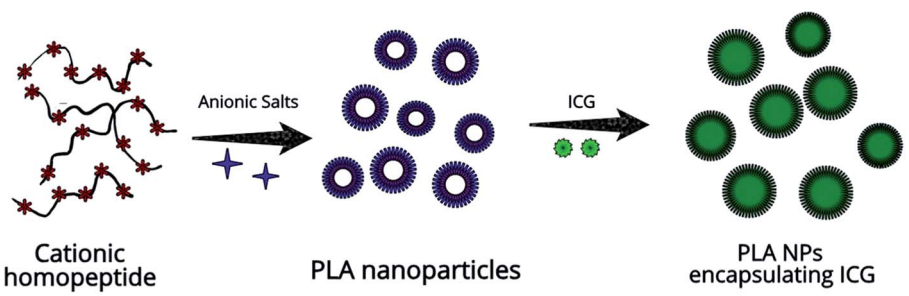

Fig. 1 Schematic representation of the ICG-PLA NPs fabrication.

equipped with 400 W xenon lamp for excitation. Fluorescence measurements were carried out in the right-angle geometry with excitation/emission slit width of 5 nm. The spectral data were collected using FluorEssence software, and origin 8.0 was used for further analysis.

Further, fluorescence lifetimes of free ICG and ICG-PLA NPs for both transitions were recorded using time-correlated single photon counting (TCSPC) instrument. For fluorescence lifetime estimation samples were excited at 405 nm by laser. The data analysis was done using IBH DAS-6 decay analysis software, and the χ^2 test was used to evaluate the goodness of the fitting. For these lifetime measurements, the fitting parameter χ^2 was $\leq$1.3. In addition to these, circular dichroism (CD) data were recorded using a spectropolarimeter (J-815, JASCO, Tokyo, Japan). Far-UV (180 to 250 nm) spectra were recorded at a rate of 20 nm per-min. Measurements of the aqueous samples were taken in a quartz cuvette of 2 mm path length and a slit width of 1 nm. Every spectrum was obtained by averaging three scans and was corrected by subtracting the blank spectrum (DI water). The CD measurements were done at 25 °C, which was maintained using a Peltier temperature controller. The scans were carried out on fresh PLA, anionic salts, and ICG solution, which was used for the synthesis of ICG-PLA NPs. All the spectroscopic measurements were done in a 10 × 2 mm quartz cuvette (Hellma, Muellheim/Baden, Germany).

2.4 Estimation of encapsulation efficiency (EE)

To determine the ICG loading efficiency, a batch of ICG-PLA NPs were synthesized and collected *via* centrifugation. The collected pellet was exposed to dimethyl sulfoxide (DMSO) for complete disruption of the NPs resulting in release free ICG. The encapsulation efficiency of the ICG within PLA NPs was calculated using eqn (1).

$$\mathrm{EE} = \left(\frac{\text{the concentration of ICG after disassembly of NPs}}{\text{the total concentration of ICG used for the synthesis}}\right) \times 100 \quad (1)$$

For calculation, the absorption spectra of disintegrated ICG-PLA NPs were measured at 792 nm as ICG in DMSO shows peak at 792 nm due to solvent effect. Further, the ICG concentration within these NPS was calculated by the calibration curve. The calibration curve of free ICG in DMSO is shown in the ESI Fig. S2.†

2.5 *In vitro* release study

The *in vitro* ICG release from ICG-PLA NPs was evaluated through dispersion method.[49] The sample was prepared and aliquoted in 5 tubes and then centrifuged to collect the NPs. Further 1 mL trypsin was added to the pellet of freshly prepared NPs at a concentration of 250 μg mL^{-1}, and the samples were incubated at 37 °C. At different time interval, the samples were centrifuged, and the absorbance of the supernatant was measured at 778 nm using UV-Vis-NIR spectrophotometer to quantify ICG release. The NPs were then placed back into the same incubation conditions. The release of ICG form PLA NPs was monitored over 24 hours. The amount of released ICG was calculated using eqn (2).

$$\text{Cumulative\% release} = \left\{\frac{\text{absorption of supernatant after every time point}}{\text{the total concentration of ICG used for the synthesis}}\right\} \times 100 \quad (2)$$

The amount of released ICG was determined by measuring the intensity of the absorbance (778 nm) using free ICG as the standard. The ICG release experiments were performed in triplicate, and the results presented are the average data over 24 hours.

2.6 Stability assessment of the ICG-PLA NPs

The optical stability of the aqueous solution of free ICG at physiological temperature is poor. The optical stability of free ICG and ICG-PLA NPs were measured under physiological conditions where both the samples were incubated in the incubator (37 °C) over a period of 72 hours in ambient light exposure. At different time points, the absorbance of ICG-PLA NPs and free ICG was measured by UV-Vis-NIR spectrophotometer. Further, to study the leakage of ICG from ICG-PLA NPs, the nanoparticles were exposed to the cell culture media at physiological temperature.

2.7 Cell culture

Cellular studies were performed on the human cervical cancer cell lines (HeLa). HeLa cells were grown and maintained in DMEM media supplemented with 10% FBS and 100 units per mL penicillin–streptomycin. Cells were incubated at 37 °C with 5% carbon dioxide (CO_2). The cells with ~80% confluency were subcultured after detaching with 0.25% trypsin–EDTA. For cellular viability assessment, HeLa cells were plated in 96 well plates with seeding density 5000 cells per well in triplicate. After incubation of 24 hours, the treatment of NPs were given to the two different sets of triplicate and were allowed to incubate for 24 hours at 37 °C. To nullify the effect of ICG absorbance at 570 nm one set of ICG-PLA NPs treated cells was not exposed to MTT, however, the fresh media was added when MTT was added to another set at a concentration of 0.5 mg mL^{-1}. After 4 hours incubation, the media was removed, 200 μL DMSO was added to the wells. The absorbance of the dissolved formazan was quantified at 570 nm by using a UV-Vis microplate reader (SynergyH1, BioTek). Cell viability was calculated by eqn (3). As a percentage decrease in viability with respect to untreated cells. Where *A* is absorbance.

$$\text{Viability}\% = \left(\frac{\text{A of NPs treated cells with MTT treatment} - \text{A of NPs treated cells without MTT}}{\text{A of control cells with MTT treatment} - \text{A of control cells without MTT}}\right) \times 100 \quad (3)$$

Cellular imaging was done on a multiphoton imaging system. HeLa cells were cultured as mention above, trypsinized, and seeded onto coverslips in a six-well plate ($\sim 2 \times 10^5$ cells per well) and were allowed to adhere for 24 hours. For the experiment, the media was removed and replaced with ICG-PLA NPs and free ICG containing cell culture media. The control cells (untreated cells) were treated with the cell culture media only. All the samples were incubated for 4 hours in an incubator. Following incubation, the media was removed, and cells were washed with 1× PBS thrice. Cell fixation was done with 4% paraformaldehyde for 30 min at room temperature, and slides were prepared with the help of mounting media for visualization under microscopy. The multiphoton imaging experiment was performed on a laser scanning MP confocal system (Olympus, FV1000, Japan). The MP confocal imaging system is equipped with the femtosecond-based negative chirped infrared laser. A mode-locked Ti-Sapphire laser (Mai Tai, DeepSee, Spectra-Physics) was used as an excitation light source, which provides approximately 70 fs pulse width at 80 MHz repetition rate with wavelengths ranging from 690 to 1064 nm. Cellular 2P imaging of the free and nanoencapsulated ICG treated cells were recorded using non-descanned detectors (NDD), which allows 575–630 nm wavelength ranges to pass (collection window of $S_2 \rightarrow S_0$ state transition of ICG).

3 Result and discussions

Effect of ICG nanoencapsulation on 2P fluorescence cellular imaging is studied. For this purpose, we have used PLA, a biocompatible and biodegradable cationic peptide, to encapsulate ICG.

3.1 Fabrication and characterization of the ICG-PLA NPs

The ICG-PLA NPs were fabricated through a simple self-assembly process in an aqueous solution without any organic solvent. A complete green chemistry-based fabrication process was used for this synthesis. As shown in Fig. S1,† an aqueous solution of PLA was mixed with the salt solution followed by the addition of free ICG, this results in the initiation of the self-assembly process and the fabrication of ICG-PLA NPs. The morphological characterization was done *via* FESEM and DLS. Fig. 2(a) shows the FESEM images of the fabricated NPs, these NPs have a spherical shape with a mean diameter of ~61 nm as shown in Fig. 2(b).

The DLS study shows that ICG-PLA NPs have a mean hydrodynamic diameter of ~154 nm shown in Fig. 2(c). The polydispersity index (PDI) was found to be 0.23, which suggests that these NPs were monodisperse in aqueous solution. The difference between the mean diameter in the dry state (SEM measurements) and aqueous state (DLS measurements) could be attributed to the shrinkage of NPs in the dry state. The zeta potential of these NPs was found to be −41.64 mV, which shows the stability of the NPs in the aqueous solution and ICG-PLA NPs will not aggregate in the aqueous environment.

3.2 Optical characterization of the free ICG and ICG-PLA NPs

The effect of nanoencapsulation of the ICG on its optical properties is shown in Fig. 3. The aqueous solution of free ICG has two major absorption peaks at 780 nm with a shoulder peak at 710 nm and at 400 nm, respectively, as shown in Fig. 3(a). Fig. 3(b) shows the Jablonski diagram depicting the possible excitation and emission transitions from and to S_0 state to higher excited states. Absorption of 780 nm and 400 nm wavelength photons leads to the transition of ICG electrons from $S_0 \rightarrow S_1$ and $S_0 \rightarrow S_2$ states, respectively. Following excitation, ICG releases their energy in the form of the fluorescence emission *via* the transition of electrons from $S_1 \rightarrow S_0$ and $S_2 \rightarrow S_0$ states respectively, as shown in the Jablonski diagram. Due to $S_2 \rightarrow S_0$ state transition ICG can be included in the list of molecules that violate Kasha's rule. In comparison with the absorption spectrum of free ICG, the nanoencapsulated ICG showed significant suppression of the 780 nm peak with a line broadening without any shift in peak position as shown in Fig. 3(a).

However, a minor increase in the absorption at 400 nm is observed in ICG-PLA NPs, which could be highly advantageous for 2P excitation to the S_2 state. The fluorescence emission of free and nanoencapsulated ICG is shown in Fig. 3(c). This is attributed to the transition of electrons from S_1 state to S_0 state. The nanoencapsulated ICG shows a significant reduction in the fluorescence emission peak at 800 nm without any peak shift. The fluorescence emission spectra of the free and nanoencapsulated ICG upon 420 nm excitation is shown in Fig. 3(d), this is attributed to the transition of electrons from S_2 state to S_0 state. Generally, upon 420 nm excitation, the fluorescence spectra of free ICG and ICP-PLL NPs showed a significant water Raman scattering peak (Fig. S3 in ESI†), however, in Fig. 3(d) we have shown the emission data after deconvoluting the water Raman scattering peak for improved clarity. This data was further smoothened using Savitzky–Golay method. As seen in Fig. 3(d), the nanoencapsulated ICG shows a decrease in emission intensity with a redshifted peak position in comparison with free ICG emission. It has been shown in the past that ICG emission gets quenched when it is in a bound state,[50] due to energy resonance transfer among the bound fluorochromes. Similarly, here ICG fluorescence gets quenched during nanoencapsulation of the ICG within the cationic polymer based nanoparticles. However, these spectroscopic results suggest that the fluorescence emission due to $S_2 \rightarrow S_0$ state transition does not get much affected after nanoencapsulation of ICG,

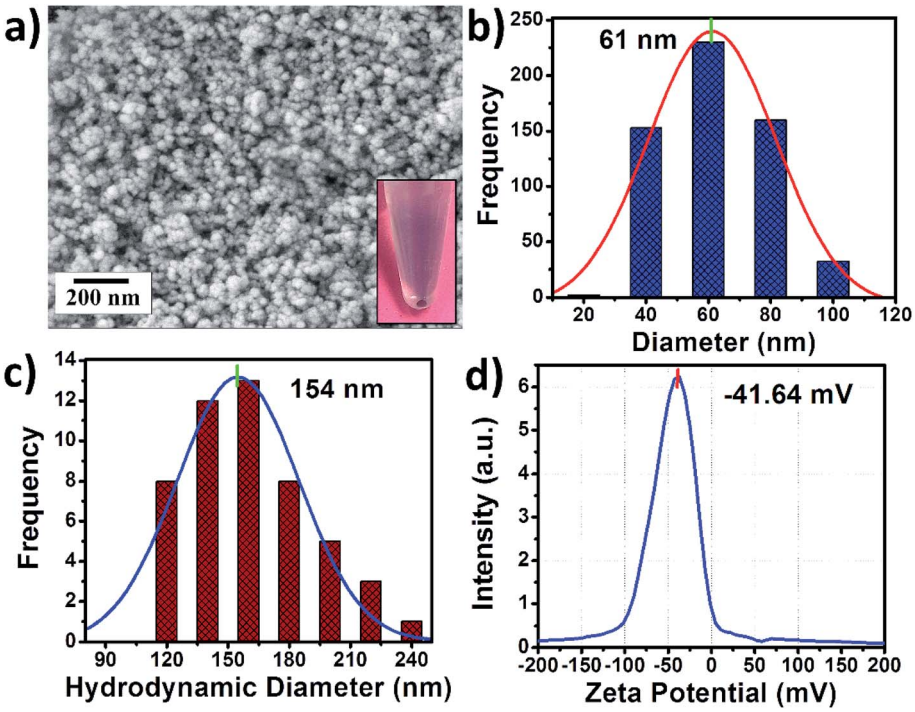

Fig. 2 Characterization of the ICG-PLA NPs encapsulating ICG (a) FESEM images; inset: a pellet of the NPs (b) frequency distribution of the particles (c) hydrodynamic diameter of the NPs (d) zeta potential of the NPs.

therefore, it might be used as an exogenous contrast agent in 2P bioimaging.

To further confirm the findings of steady-state fluorescence emission the time-resolved fluorescence measurements on free and nanoencapsulated ICG were carried out.

The fluorescence lifetime measurements of the free and nanoencapsulated ICG were measured upon 405 nm excitation. The fluorescence lifetimes of free and nanoencapsulated ICG for S_2 state were found to be 209.4 and 92 ps, respectively, as shown in Fig. 4(a). These results further confirm the quenching

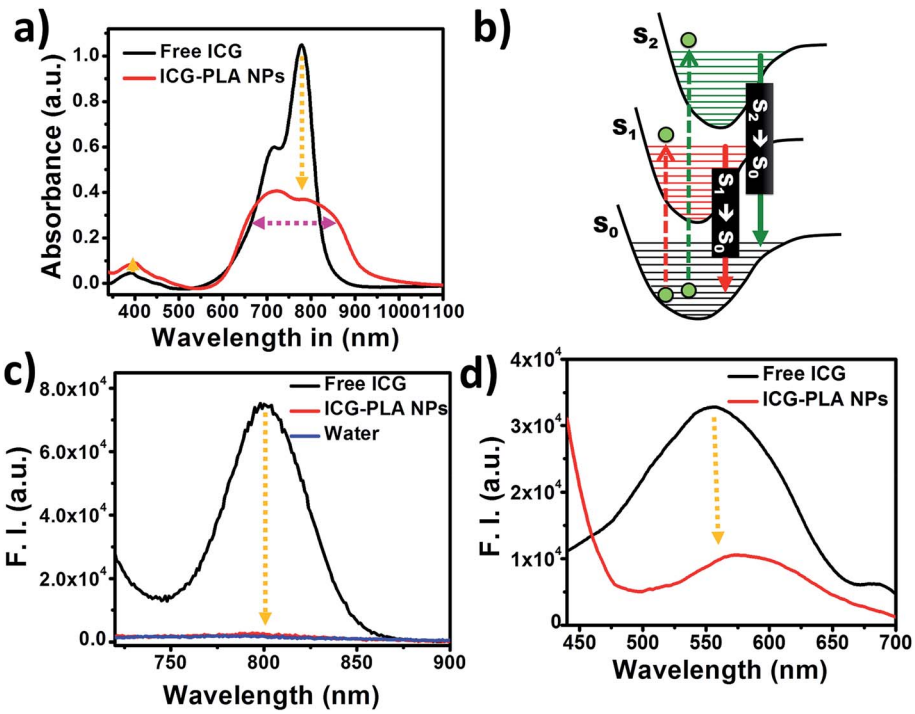

Fig. 3 Spectroscopic analysis of the free ICG and ICG-PLA NPs (a) absorption spectra (b) mechanism of possible transitions (c) fluorescence emission upon 680 nm excitation (d) fluorescence emission upon 420 nm excitation.

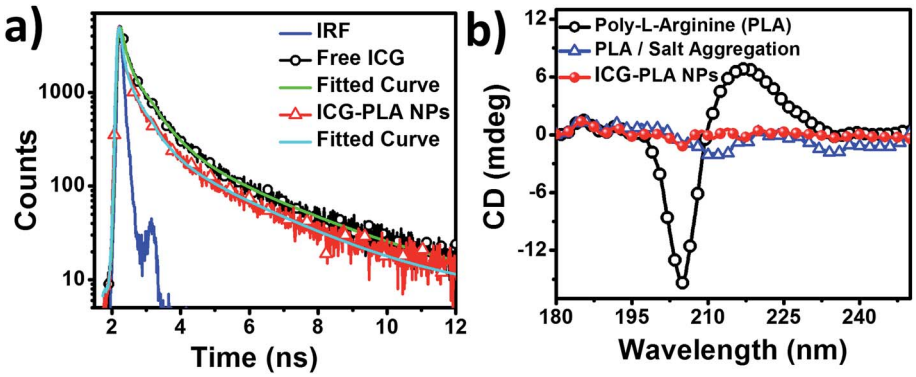

Fig. 4 Time-resolved studies and CD analysis of the free ICG and ICG-PLA NPs (a) TCSPC of the free ICG and ICG-PLA NPs at 575 nm upon 405 nm excitation (b) CD spectra of the PLA, PLA/salt and ICG-PLA NPs.

of the fluorescence emission of ICG in nanoencapsulated form. The fitting parameter χ^2 was ≤1.3 for all the fitting. To further understand the role of ICG on the stability of the NPs, circular dichroism (CD) measurements were carried out. Fig. 4(b) shows the CD spectra of aqueous PLA, PLA and salt aggregates, and ICG-PLA NPs. The CD spectra of an aqueous solution of PLA exhibits one negative peak at ~204 nm and one positive peak at ~217 nm. This suggests the presence of a random structure of PLA homopeptide in the aqueous solution as shown in Fig. 4(b). PLA CD spectral alterations due to PLA/salt aggregation is reflected by the changes in the intrinsic CD spectrum of PLA. The peak at ~204 nm and ~217 nm got suppressed due to the interaction of PLA with salt. However, the PLA/salt aggregates have a small magnitude of two negative peaks at ~212 nm and ~236 nm, which further got suppressed after the addition of ICG. This suggests the complexation of PLA homopeptide largely depends on the amino acid residues, which function as the binding ligands for a small molecule to encapsulate. Initially, the complexation of the PLA is done with the EDTA salt at a fixed molar charge ratio (MCR, eqn (S1)†), which results in the complexation between two guanidinium groups and salt. Further, the addition of the ICG in this reaction resulted in the formation of the ICG-PLA NPs, which provides more stability to this self-assembled structure as shown by the red curve in Fig. 4(b). The CD result strongly suggests that the two-guanidinium groups of PLA, act as a ligand, which makes a complex with salt and dye to form stable NPs.

3.3 ICG release, biosafety and stability study of ICG-PLA NPs

The encapsulated ICG was shielded from any external factors, which deteriorate its optical properties in free form. However, efficient delivery of ICG to the cellular level is required for improved multiphoton imaging. Here, ICG was encapsulated within salt cross-linked PLA NPs *via* self-assembly method. However, in nanoencapsulated state, ICG emission was quenched due to energy resonance transfer among the bound fluorochromes,[50] and could be regained after enzymatically degradation of the polymer as shown in Fig. 5(a and b). The ICG release study was done in the presence of proteolytic enzyme at 37 °C. A commonly used protease enzyme trypsin was used to study the ICG release from ICG-PLA NPs. The freshly prepared NPs were incubated with 250 μg mL^{-1} of trypsin in 37 °C for 24 hours. The instant release of 43% of ICG from ICG-PLA NPs was observed upon 30 minutes of incubation. Therefore, these NPs are protease responsive, where fluorescence signal increased due to cleavage of PLA homopeptide on carboxy-terminal in the presence of the protease as depicted in Fig. 5(b). This results in small fragments of amino-acid residues,[51] salt, and free ICG.

However, within 5 hours of trypsin incubation, nearly 94% of ICG was released, followed by a 98% released after 24 hours of incubation. To explore the biomedical application of the nanoencapsulated ICG, the cellular viability of these NPs was tested using MTT assay over the range of concentration. As shown in Fig. 5(d), no significant cytotoxicity was observed even at very high concentration of these NPs. Hence, this indicates that these NPs are safe and biocompatible nanocarrier for biomedical applications.

The optical stability of the nanoencapsulated ICG is a vital parameter for bioimaging applications. Here, the optical stability of the free and encapsulated ICG in physiological conditions was monitored. It is well known that the optical properties of ICG are dependent on temperature, time, and long-term optical exposure. Due to these factors optical properties degrade gradually. The effect of optical exposure on the optical properties of free and nanoencapsulated ICG over a period of time at physiological temperature was monitored. The free ICG and ICG-PLA NPs were incubated at 37 °C for 72 hours in ambient light exposure. As shown in Fig. 6(a), the optical property of ICG-PLA NPs was found to be significantly more stable in comparison with the free ICG. The optical property of free ICG started degrading after 30 minutes of the incubation on the other hand ICG-PLA NPs were stable up to 72 hours as shown in Fig. 6(a).

The stability of ICG-PLA NPs in physiological environment was studied by incubating them in cell culture media for 24 hours at 37 °C. At different time points sample was centrifuged and the fluorescence emission of the supernatant was measured. As shown in Fig. 6(b), ICG-PLA NPs were 95% stable in the physiological condition. According to the results, ICG-PLA NPs are stable nanocarriers for ICG delivery

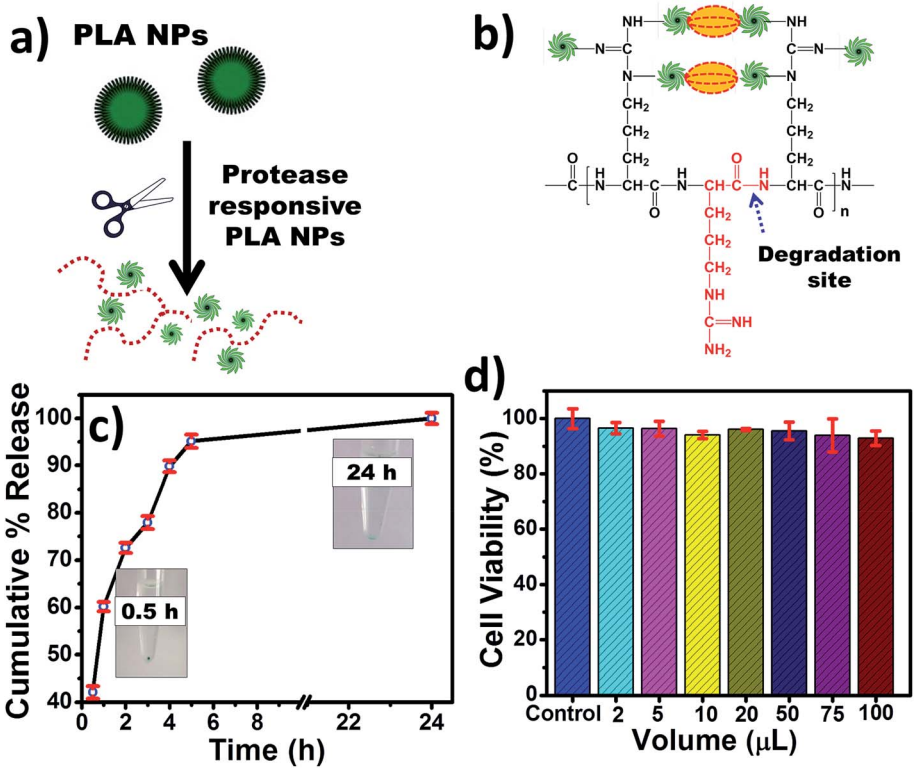

Fig. 5 Release and cellular toxicity of the ICG-PLA NPs. (a) Schematic showing the principle of the ICG-PLA NPs as a protease responsive NPs (b) mechanism of the fluorescence activation (c) *in vitro* release study over 24 h (d) cellular viability of the ICG-PLA NPs over the range.

in the cells. Additionally, the EE of the ICG was estimated by using eqn (1). The total 56% of ICG was loaded in one batch of the ICG-PLA NPs.

3.4 Multiphoton imaging

The multiphoton imaging ability of the nanoencapsulated ICG was studied after staining the HeLa cells. Previously, our group had reported the nonlinear excitation of free ICG to the S_2 state followed by its direct relaxation to S_0 state causing an emission and used for the multiphoton imaging applications.[21] However, the use of free form of ICG has limitations such as poor photostability and cellular uptake. Herein, ICG-PLA NPs were used to overcome the limitations of free ICG and its nonlinear excitation to the S_2 state followed by emission was reported for 2P bioimaging. These ICG-PLA NPs are promising vectors for intracellular drug delivery as they can be taken up by the cells *via* endocytosis.[52] Fig. 7(a) shows the bright field and 2P images of the HeLa cells treated with free ICG and ICG-PLA NPs, cells without any treatment were considered as a control. Bright field and 2P emission images due to $S_2 \rightarrow S_0$ state transition of ICG when excited by 790 nm femtosecond laser are shown in the first and second columns respectively. However, the first, second and third rows show the control, free ICG, and ICG-PLA

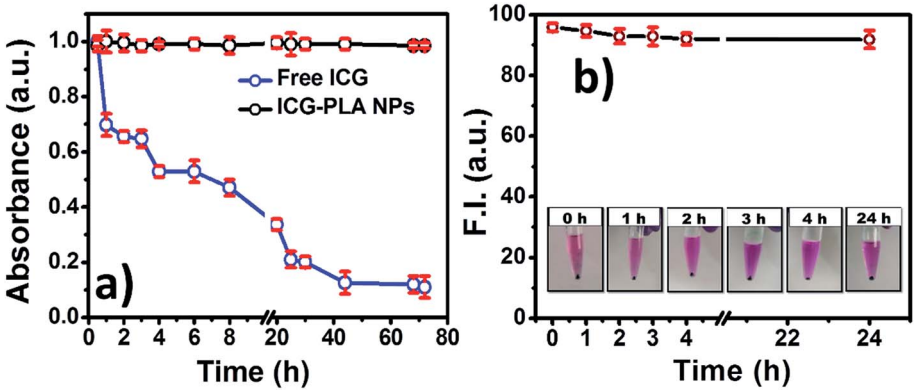

Fig. 6 Stability of the ICG-PLA NPs (a) optical stability of aqueous ICG-PLA NPs and free ICG at 37 °C (b) ICG-PLA NPs media stability over 24 h at physiological condition.

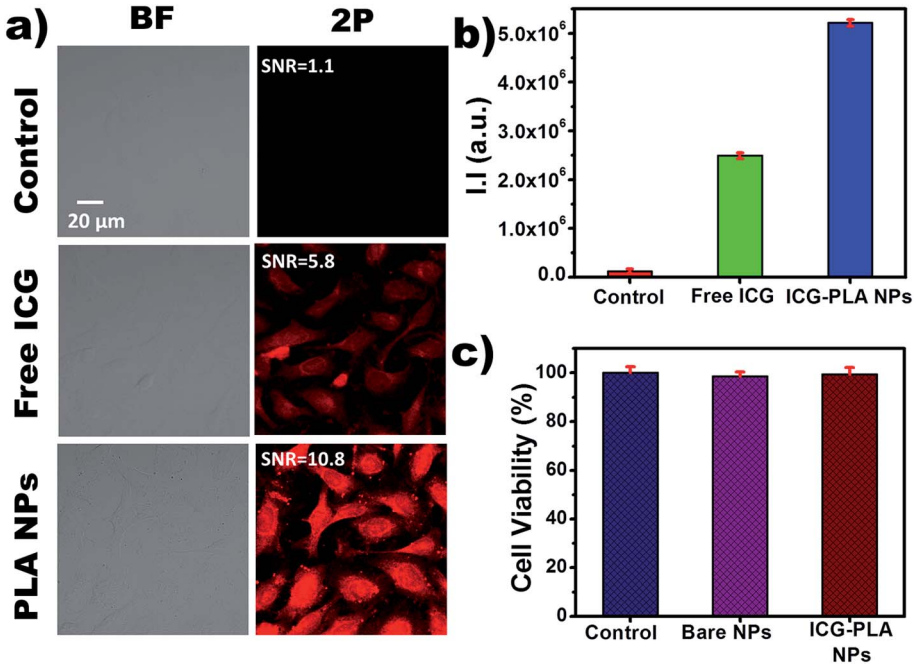

Fig. 7 Cellular uptake, localization and viability studies (a) bright field and 2P imaging of the cells by multiphoton imaging system using 40× lens with 2× zooming. (b) Integral intensity of the control, free ICG, and 2P imaging. (c) Cellular viability of the bare and ICG-PLA NPs used for the experiment. Where, I.I; integral intensity.

NPs treated cells respectively. As clearly evident by Fig. 7(a) the ICG-PLA NPs treated cells showed significantly higher emission in comparison with free ICG treated cells. These results suggest that ICG-PLA NPs are efficiently taken up by the cells in comparison with free ICG. This also indicates that the PLA NPs are highly efficient to deliver ICG to the cells and it could be attributed to PLA, which is a known cell-penetrating peptide. Additionally, the SNR ratio of the ICG-PLA NPs were higher then free ICG. Furthermore, for better quantification of the 2P ($S_2 \rightarrow S_0$ state) emission, integral fluorescence intensity was calculated using ImageJ and plotted as shown in Fig. 7(b). According to the results, the ICG-PLA NPs has showed five-fold increases in multiphoton emission than free ICG multiphoton images. For bioimaging applications, the biosafety of these nanoparticles was also assessed using cellular viability assay. For cell viability experiments untreated cells, bare PLA nanoparticle-treated cells, and ICG-PLA NPs treated cells were studied. As seen in Fig. 7(c), bare PLA nanoparticle treated, and ICG-PLA NPs treated cells show excellent biosafety with more than 98% cellular viability.

These results collectively confirmed the effectiveness of ICG-PLA NPs as a biocompatible and biodegradable exogenous contrast agent for 2P cellular imaging application.

4 Conclusion

We have successfully encapsulated ICG in a cationic homopeptide PLA and studied the application of nanoencapsulated ICG for multiphoton imaging. The nanoparticle synthesis was performed by a simple two-step self-assembly process in an aqueous environment without using any organic solvent. It was found that ICG-PLA NPs exhibit excellent biosafety, they show no observable toxicity to the cells at tested concentrations. These NPs can be used as a highly efficient and biologically safe exogenous multiphoton contrast agent with remarkably improved photostability in comparison to free ICG. The ICG-PLA NPs show surprisingly high cellular uptake. These NPs are fabricated using homopeptide of arginine, which is a semi-essential amino acid and is likely to be degraded in the body.

Conflicts of interest

There are no conflicts to declare.

Acknowledgements

The authors of this work would like to acknowledge sophisticated instrumentation laboratory (SIC) of Indian Institute of Technology Indore for providing various characterization techniques. Further, the authors would like to thanks Dr Tridib Sarma and Siddarth Jain for DLS measurements. Ms. Anshu Kumari would like to thank Department of Science and Technology (DST), Government of India, for providing fellowship under INSPIRE Fellowship (DST/INSPIRE Fellowship/2014/IF140809).

References

1 D. B. Kopans, Updated results of the trials of screening mammography, *Surg. Oncol. Clin. N. Am.*, 1997, **6**(2), 233–263.

2 W. K. Moon, Y. Lin, T. O'Loughlin, Y. Tang, D. E. Kim, R. Weissleder and C. H. Tung, Enhanced tumor detection using a folate receptor-targeted near-infrared fluorochrome conjugate, *Bioconjugate Chem.*, 2003, **14**(3), 539–545.

3 A. Becker, C. Hessenius, K. Licha, B. Ebert, U. Sukowski, W. Semmler, B. Wiedenmann and C. Grötzinger, Receptor-targeted optical imaging of tumors with near-infrared fluorescent ligands, *Nat. Biotechnol.*, 2001, **19**(4), 327–331.

4 C. H. Tung, S. Bredow, U. Mahmood and R. Weissleder, Preparation of a cathepsin D sensitive near-infrared fluorescence probe for imaging, *Bioconjugate Chem.*, 1999, **10**(5), 892–896.

5 B. Ballou, G. W. Fisher, T. R. Hakala and D. L. Farkas, Tumor detection and visualization using cyanine fluorochrome-labeled antibodies, *Biotechnol. Prog.*, 1997, **13**(5), 649–658.

6 D. W. Piston, Imaging living cells and tissues by two-photon excitation microscopy, *Trends Cell Biol.*, 1999, **9**(2), 66–69.

7 W. B. Amos, J. G. White and M. Fordham, Use of confocal imaging in the study of biological structures, *Appl. Opt.*, 1987, **26**(16), 3239–3243.

8 P. T. C. So, C. Y. Dong, B. R. Masters and K. M. Berland, Two-photon excitation fluorescence microscopy, *Annu. Rev. Biomed. Eng.*, 2000, **02**, 399–429.

9 W. Denk, J. H. Strickler and W. W. Webb, Two-photon laser scanning fluorescence microscopy, *Science*, 1990, **248**(4951), 73–76.

10 S. Yazdanfar, C. Joo, C. Zhan, M. Y. Berezin, W. J. Akers and S. Achilefu, Multiphoton microscopy with near infrared contrast agents, *J. Biomed. Opt.*, 2010, **15**(3), 030505.

11 C. Shirata, J. Kaneko, Y. Inagaki, T. Kokudo, M. Sato, S. Kiritani, N. Akamatsu, J. Arita, Y. Sakamoto, K. Hasegawa and N. Kokudo, Near-infrared photothermal/photodynamic therapy with indocyanine green induces apoptosis of hepatocellular carcinoma cells through oxidative stress, *Sci. Rep.*, 2017, **7**(1), 1–8.

12 S. Luo, E. Zhang, Y. Su, T. Cheng and C. Shi, A review of NIR dyes in cancer targeting and imaging, *Biomaterials*, 2011, **32**(29), 7127–7138.

13 C. M. Leevy, C. L. Mendenhall, W. Lesko and M. M. Howard, Estimation of hepatic blood flow with indocyanine green, *J. Clin. Invest.*, 1962, **41**(5), 1169–1179.

14 M. Haruna, K. Kumon, N. Yahagi, Y. Watanabe, Y. Ishida, N. Kobayashi and T. Aoyagi, Blood volume measurement at the bedside using ICG pulse spectrophotometry, *Anesthesiology*, 1998, **89**(6), 1322–1328.

15 R. C. Benson and H. A. Kues, Fluorescence properties of indocyanine green as related to angiography, *Phys. Med. Biol.*, 1978, **23**(1), 159–163.

16 D. Jarrar, P. Wang, G. Y. Song, M. W. Knoferl, W. G. Cioffi, K. I. Bland and I. H. Chaudry, Metoclopramide: a novel adjunct for improving cardiac and hepatocellular functions after trauma-hemorrhage, *Am. J. Physiol.: Endocrinol. Metab.*, 2000, **278**(1), E90–E95.

17 G. S. Jayabalan, Y. Wu, J. F. Bille, S. Kim, X. W. Mao, H. V Gimbel, M. E. Rauser and J. T. Fan, In vivo two-photon imaging of retina in rabbits and rats Gopal, *Exp. Eye Res.*, 2018, **166**, 40–48.

18 Y. Pu, L. Shi, S. Pratavieira and R. R. Alfano, "Two-photon excitation microscopy using the second singlet state of fluorescent agents within the 'tissue optical window, *J. Appl. Phys.*, 2013, **114**(2013), 153102.

19 M. Beer and H. C. Longuet-Higgins, Anomalous light emission of azulene, *J. Chem. Phys.*, 1955, **23**(8), 1390–1391.

20 M. Kasha, Characterization of electronic transitions in complex molecules, *Discuss. Faraday Soc.*, 1950, **9**, 14–19.

21 A. Kumari and S. Gupta, Two-photon excitation and direct emission from S_2 state of U.S. Food and Drug Administration approved near-infrared dye: application of anti-Kasha's rule for two-photon fluorescence imaging, *J. Biophotonics*, 2018, e201800086.

22 K. Park, S. Lee, E. Kang, K. Kim, K. Choi and I. C. Kwon, New generation of multifunctional nanoparticles for cancer imaging and therapy, *Adv. Funct. Mater.*, 2009, **19**(10), 1553–1566.

23 W. S. Kuo, Y. T. Chang, K. C. Cho, K. C. Chiu, C. H. Lien, C. S. Yeh and S. J. Chen, Gold Nanomaterials Conjugated with Indocyanine Green for Dual-Modality Photodynamic and Photothermal Therapy, *Biomaterials*, 2012, **33**(11), 3270–3278.

24 H. Gao, O. A. Goriacheva, N. V. Tarakina and G. B. Sukhorukov, Intracellularly Biodegradable Polyelectrolyte/Silica Composite Microcapsules as Carriers for Small Molecules, *ACS Appl. Mater. Interfaces*, 2016, **8**(15), 9651–9661.

25 H. Chen and S. He, PLA-PEG coated multifunctional imaging probe for targeted drug delivery, *Mol. Pharm.*, 2015, **12**(6), 1885–1892.

26 Y.-Y. Ma, K.-T. Jin, S.-B. Wang, H.-J. Wang, X.-M. Tong, D.-S. Huang and X.-Z. Mou, Molecular Imaging of Cancer with Nanoparticle-Based Theranostic Probes, *Contrast Media Mol. Imaging*, 2017, **2017**, 1–11.

27 S. Plianwong, P. Opanasopit, T. Ngawhirunpat and T. Rojanarata, Chitosan combined with poly-l-arginine as efficient, safe, and serum-insensitive vehicle with RNase protection ability for siRNA delivery, *BioMed Res. Int.*, 2013, **2013**(574136), 1–9.

28 Y. A. Guerrero, B. Bahmani, S. P. Singh, V. I. Vullev, V. Kundra and B. Anvari, Virus-resembling nano-structures for near infrared fluorescence imaging of ovarian cancer HER2 receptors, *Nanotechnology*, 2015, **26**(1–10), 453102.

29 B. Jung, A. L. N. Rao and B. Anvari, Optical Nano-Constructs Composed of Genome- Depleted Brome Mosaic Virus Doped with a Near Infrared Chromophore for Potential Biomedical Applications, *ACS Nano*, 2011, **5**(1), 1–8.

30 H. G. Bagaria and M. S. Wong, Polyamine–salt aggregate assembly of capsules as responsive drug delivery vehicles, *J. Mater. Chem.*, 2011, **21**(26), 9454.

31 G. Kim, S.-W. Huang, K. C. Day, M. O'Donnell, R. R. Agayan, M. A. Day, R. Kopelman and S. Ashkenazi, Indocyanine-green-embedded PEBBLEs as a contrast agent for photoacoustic imaging, *J. Biomed. Opt.*, 2007, **12**(4), 044020.

32 R. Manchanda, A. Fernandez-Fernandez, A. Nagesetti and A. J. McGoron, Preparation and characterization of a polymeric (PLGA) nanoparticulate drug delivery system

with simultaneous incorporation of chemotherapeutic and thermo-optical agents, *Colloids Surf., B*, 2010, **75**(1), 260–267.

33 Z. Niu, E. Tedesco, F. Benetti, A. Mabondzo, I. M. Montagner, I. Marigo, D. Gonzalez-Touceda, S. Tovar, C. Diéguez, M. J. Santander-Ortega and M. J. Alonso, Rational design of polyarginine nanocapsules intended to help peptides overcoming intestinal barriers, *J. Controlled Release*, 2017, **263**, 4–17.

34 J. R. Vanegas Sáenz, T. Tenkumo, Y. Kamano, H. Egusa and K. Sasaki, Amiloride-enhanced gene transfection of octa-arginine functionalized calcium phosphate nanoparticles, *PLoS One*, 2017, **12**(11), 1–15.

35 T. Yamaki, M. Uchida, Y. Kuwahara, Y. Shimazaki, K. Ohtake, M. Kimura, H. Uchida, J. Kobayashi, M. Ogihara, Y. Morimoto and H. Natsume, Effect of poly-L-arginine on intestinal absorption of hydrophilic macromolecules in rats, *Biol. Pharm. Bull.*, 2013, **36**(3), 496–500.

36 H. C. Bygd, D. Akilbekova, A. Muñoz, K. D. Forsmark and K. M. Bratlie, Poly-l-arginine based materials as instructive substrates for fibroblast synthesis of collagen, *Biomaterials*, 2015, **63**, 47–57.

37 S. Futaki, Arginine-rich peptides: potential for intracellular delivery of macromolecules and the mystery of the translocation mechanisms, *Int. J. Pharm.*, 2002, **245**(1–2), 1–7.

38 Y. Kamiya, T. Yamaki, M. Uchida, T. Hatanaka, M. Kimura, M. Ogihara, Y. Morimoto and H. Natsume, Preparation and Evaluation of PEGylated Poly-L-ornithine Complex as a Novel Absorption Enhancer, *Biol. Pharm. Bull.*, 2017, **40**(2), 205–211.

39 J. B. Rothbard, S. Garlington, Q. Lin, T. Kirschberg, E. Kreider, P. L. McGrane, P. A. Wender and P. A. Khavari, Conjugation of arginine oligomers to cyclosporin A facilitates topical delivery and inhibition of inflammation, *Nat. Med.*, 2000, **6**(11), 1253–1257.

40 S. Sasidharan, D. Bahadur and R. Srivastava, Protein-Poly(amino acid) Nanocore-Shell Mediated Synthesis of Branched Gold Nanostructures for Computed Tomographic Imaging and Photothermal Therapy of Cancer, *ACS Appl. Mater. Interfaces*, 2016, **8**(25), 15889–15903.

41 A. Pensado, F. J. Diaz-Corrales, B. De la Cerda, L. Valdés-Sánchez, A. A. del Boz, D. Rodriguez-Martinez, A. B. García-Delgado, B. Seijo, S. S. Bhattacharya and A. Sanchez, Span poly-L-arginine nanoparticles are efficient non-viral vectors for PRPF31 gene delivery: an approach of gene therapy to treat retinitis pigmentosa, *Nanomedicine*, 2016, **12**(8), 2251–2260.

42 D. S. Lind, Arginine and Cancer, *J. Nutr.*, 2004, **134**(10), 2837S–2841S.

43 F. Tanvir, A. Yaqub, S. Tanvir and W. Anderson, Poly-L-arginine Coated Silver Nanoprisms and their Anti-Bacterial Properties, *Nanomaterials*, 2017, **7**(10), 296.

44 S. Kudo and Y. Nagasaki, A novel nitric oxide-based anticancer therapeutics by macrophage-targeted poly(l-arginine)-based nanoparticles, *J. Controlled Release*, 2015, **217**, 256–262.

45 M. Sepahi, R. Jalal and M. Mashreghi, Antibacterial activity of poly-l-arginine under different conditions, *Iran J. Microbiol.*, 2017, **9**(2), 103–111.

46 J. Z. S. Chiu, I. G. Tucker, B. J. McLeod and A. McDowell, Arginine-tagging of polymeric nanoparticles via histidine to improve cellular uptake, *Eur. J. Pharm. Biopharm.*, 2015, **89**, 48–55.

47 H. J. Cho, S. Chong, S. J. Chung, C. K. Shim and D. D. Kim, Poly-L-arginine and dextran sulfate-based nanocomplex for epidermal growth factor receptor (EGFR) siRNA delivery: its application for head and neck cancer treatment, *Pharm. Res.*, 2012, **29**(4), 1007–1019.

48 M. V. Lozano, G. Lollo, M. Alonso-Nocelo, J. Brea, A. Vidal, D. Torres and M. J. Alonso, Polyarginine nanocapsules: a new platform for intracellular drug delivery, *J. Nanopart. Res.*, 2013, **15**(1515), 1–14.

49 G. Shazly, T. Nawroth and P. Langguth, Comparison of Dialysis and Dispersion Methods for in vitro Release Determination of Drugs from Multilamellar Liposomes, *Dissolution Technol.*, 2008, 7–10.

50 C. H. Tung, U. Mahmood, S. Bredow and R. Weissleder, In vivo imaging of proteolytic enzyme activity using a novel molecular reporter, *Cancer Res.*, 2000, **60**(17), 4953–4958.

51 X. R. Zhao, Y. L. Chen, L. Wang, W. F. Wang and X. G. Chen, Highly sensitive fluorescence detection of trypsin based on gold nanoparticle probes, *Anal. Methods*, 2016, **8**(2), 393–400.

52 T. Yamaki, Y. Kamiya, K. Ohtake, M. Uchida, T. Seki, H. Ueda, J. Kobayashi, Y. Morimoto and H. Natsume, A mechanism enhancing macromolecule transport through paracellular spaces induced by poly-L-arginine: poly-L-arginine induces the internalization of tight junction proteins via clathrin-mediated endocytosis, *Pharm. Res.*, 2014, **31**(9), 2287–2296.

